ADVANCED MATERIALS

Supporting Information

for *Adv. Mater.,* DOI: 10.1002/adma.201805405

A Highly Active Star Decahedron Cu Nanocatalyst for Hydrocarbon Production at Low Overpotentials

*Chungseok Choi, Tao Cheng, Michelle Flores Espinosa, Huilong Fei, Xiangfeng Duan, William A. Goddard III, and Yu Huang**

Supporting Information

A Highly Active Star Decahedron Cu Nanocatalyst for Hydrocarbon Production at Low Overpotentials

Chungseok Choi, Tao Cheng, Michelle Flores Espinosa, Huilong Fei, Xiangfeng Duan, William A. Goddard III, Yu Huang*

Chemicals: Copper(II) acetylacetonate ($Cu(acac)_2$, 99.9%), L-Ascorbic acid (> 99%), Oleylamine (OAm) (> 70%), Ethanol (200 proof), were all purchased from Sigma-Aldrich. The deionized (DI) water (18.2 MΩ cm^{-1}) used in aqueous solutions was prepared by using ultra-pure purification system (Aqua Solutions).

Preparation of star decahedron Cu nanoparticle (SD-Cu NPs) catalyst: We used oleylamine (OAm) as capping agent and solvent; L-Ascorbic acid serves as reducing agent and $Cu(acac)_2$ is the precursor. In a typical synthesis of SD-Cu NPs catalyst, $Cu(acac)_2$ (11 mg), L-Ascorbic acid (52.6 mg) were pre-dissolved in OAm (5 mL) containing 30 ml vial. The mixture was sonicated for 15 min and transferred to an oil bath. The oil bath was heated at 130 °C for 4 hr and cooled to room temperature. The synthesized colloidal products were washed five times with hexane/ethanol solvents and collected by centrifuge at 9500 rpm.

Materials characterizations: TEM samples were prepared by dropping and drying ethanol dispersion of catalysts onto carbon-coated copper TEM grids (Ted Pella, Redding, CA) under room temperature. Transmission electron microscopy (TEM) images were taken on an FEI CM120 transmission electron microscope operated at 120 kV. High-resolution TEM images (HRTEM) were carried out on an FEI Titan transmission electron microscope operated at 300 kV. The size of SD-Cu NPs was measured by the longest distance from one corner to one center of the edge. Powder X-ray diffraction (PXRD) patterns were analyzed with a Panalytical X'Pert Pro X-ray Powder Diffractometer with Cu-Kα radiation. Ultraviolet photoelectron spectroscopy (UPS) tests were conducted on Kratos AXIS Ultra DLD spectrometer. To make sure UPS data, we analyzed Cu(100) foil and d-band of Cu(100), which are well matched with the d-band shape of Cu(100) foil compared to a published paper[1]; Cu 4s band around 9 eV, d-band starting 1.94 eV below Fermi level, 2.62 d-band widths and higher intensity at the leading edge as included in Figure S10.[2] The Shirley background was subtracted to calculate the d-band center. The concentration of catalysts was measured by inductively coupled plasma atomic emission spectroscopy (TJA RADIAL IRIS 1000 ICP-AES).

Electrochemical Measurements: Current densities were measured by using a three-electrode cell. A glassy-carbon Rotating Disk Electrode (RDE) (diameter: 5 mm, area: 0.196 cm^2) from Pine Instruments was used as a working electrode. Consumed charges for calculating faradaic efficiency (FE) was collected by using a gas-tight electrolysis H cell (Pine research) separated with anion exchange membrane from Princeton Applied Research VersaSTAT 4 workstation. In a typical setup, 1x1 cm^2 glassy-carbon electrode, Ag/AgCl (1 M KCl) electrode, and Pt wire electrode were used as working, reference and counter electrode respectively. Every electrochemical CO_2RR was conducted with the 0.1 M $KHCO_3$ electrolyte solution. CO_2 (Air gas, 99.999%) was bubbled for 30 minutes before CO_2RR; CO_2 was continuously purged into the cathodic compartment at 10 sccm. Cyclic voltammetry (CV) was performed in CO_2-saturated 0.1 M $KHCO_3$ electrolyte with a potential scan rate of 5 mV s^{-1}. All discussed potentials were converted to those against reversible hydrogen electrode (RHE) after iR corrected during the measurement.

Product analysis: An outlet gas line from the gas-tight H cell was directly routed to a p-type Hastelloy 6 port sampling loop (1.5 ml). A data point was obtained after applied a constant potential for 35 ± 1 min. 1.5 ml effluence gas was analyzed on Shimadzu Tracera GC-BID 2010Plus (Shimadzu) equipped with a Restek Micropacked GC column every 35 ± 1 min. The GC-BID detector was calibrated by two standard gases and two different sampling volumes (20 µl and 1.5 ml). Helium was used as the carrier gas (Air gas, 99.9999%). The FE was calculated as below:[3]

$$FE_J = \frac{2Fv_J Gp_0}{RT_0 i_{total}} \times 100\%$$

where:

v_J (vol%) = volume concentration of gas products in the effluence gas from the electrochemical cell (GC data)

G (ml min^{-1} at room temperature and ambient pressure) = Gas flow rate measured by a ProFlow 6000 electronic flow meter (Restek) at the exit of the electrochemical cell

i_{total} (mA) = steady-state cell current

p_0=1.01 x 105 Pa, T_0= 298.15 K, F = 96485 C•mol^{-1}, R = 8.314 J• mol^{-1}• K^{-1}

The liquid product was analyzed by quantitative NMR (Bruker AV-600). For instance, 0.9 mL of the reacted electrolyte was mixed with D_2O (0.1 mL), and 10 µl of dimethyl sulfoxide (25 mM) was added to the mixture as an internal standard. The 1D ^1H spectrum was measured with a pre-water saturation method.

Electrochemically active surface area (ECSA): The electrochemically active surface area (ECSA) measurements were carried out by lead (Pb) under-potential deposition (UPD). The ECSA was determined by subtracting the background current from integrating the Pb desorption charge on the CV at room temperature in nitrogen saturated $HClO_4$ (0.1 M) + $Pb(ClO_4)_2$ solution (0.001 M).[4]

Computational details: The quantum mechanics (QM) calculations were carried out using the VASP software at the version of 5.4.4,[5-7] with the Perdew, Burke, and Ernzerhof (PBE) flavor[8] of density functional theory (DFT). The projector augmented wave (PAW) method[9] was used to account for core-valence interactions. The kinetic energy cutoff for plane wave expansions was set to 400 eV, and reciprocal space was sampled by the Γ-centered Monkhorst-Pack scheme with a grid of 3×3×1. The vacuum layer is at least 15 Å above the surface. The convergence criteria are 1×10^{-7} eV energy differences for solving the electronic wave function. The Methfessel-Paxton smearing of second order with a width of 0.1 eV was applied. All geometries (atomic coordinates) were converged to within 1×10^{-2} eV $Å^{-1}$ for maximal components of forces. A post-stage vdW DFT-D3 method with Becke-Jonson damping was applied.[10]

The Gibbs free energies were calculated at 298 K and 1 atm as outlined in (S1):

$$G = H - T \Delta S = E_{DFT} + E_{ZPE} + E_{solv} + \int_0^{298} C_V dT - T \Delta S \quad \text{(S1)}$$

Where E_{DFT} is the DFT-optimized total energy, E_{ZPE} is the zero-point vibrational energy, E_{solv} is the solvation energy. $\int_0^{298} C_V dT$ is the heat capacity, T is the temperature, and ΔS is the entropy. Gas-phase molecules such as CO were treated using the ideal gas approximation, whereas adsorbents were treated using a harmonic approximation. The solvation was treated implicitly using the CANDLE method[11] using the JDFTx simulation package. The GBRV[12] ultrasoft pseudopotentials (USPP) were used, with a plane wave cutoff of 544 eV (20 a.u.). All other settings are similar to those in VASP calculations.

Supporting Figures and Tables

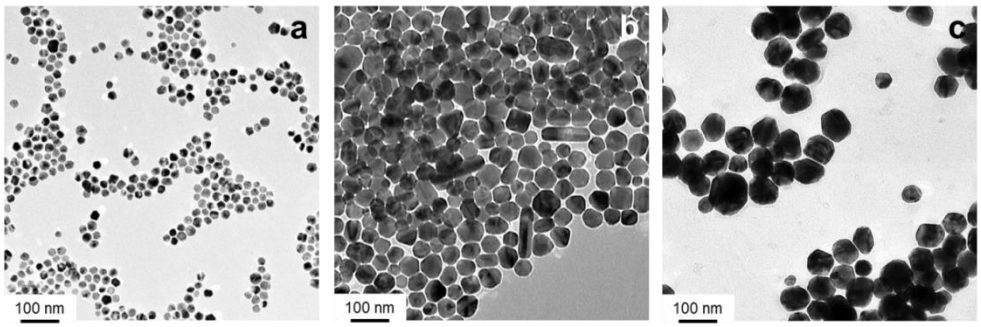

Figure S1. Low magnification TEM images of Cu NPs by different reaction temperatures, (a) synthesis of Cu NPs with Cu $(acac)_2$/oleylamine (0.22 mg/ml) at 130 °C, (b) synthesis of Cu NPs with Cu $(acac)_2$/oleylamine (0.22 mg/ml) at 150 °C, (c) synthesis of Cu NPs with Cu $(acac)_2$/oleylamine (0.22 mg/ml) at 170 °C.

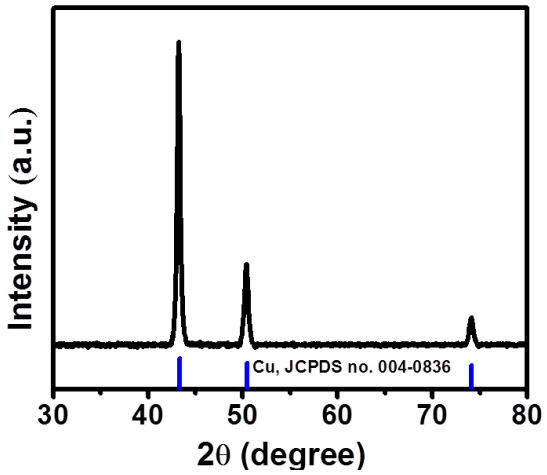

Figure S2. PXRD of SD-Cu NPs.

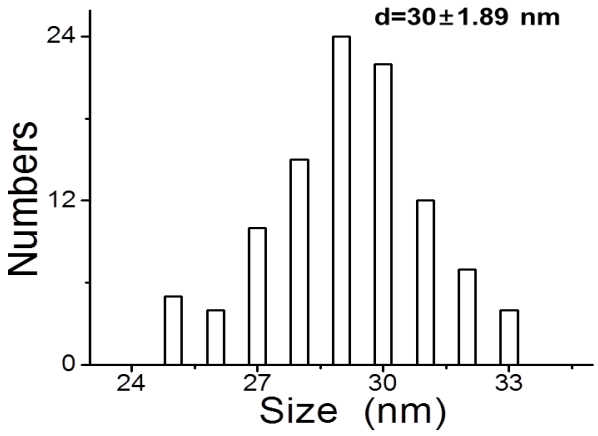

Figure S3. Size distribution of SD-Cu NPs.

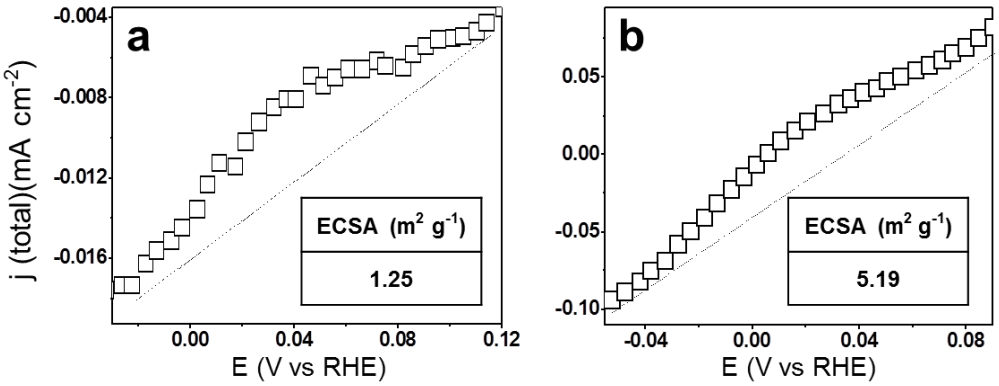

Figure S4. Measurement of ECSA by using a Pb under potential method, (a) SD-Cu NPs, (b) PC-Cu NPs.

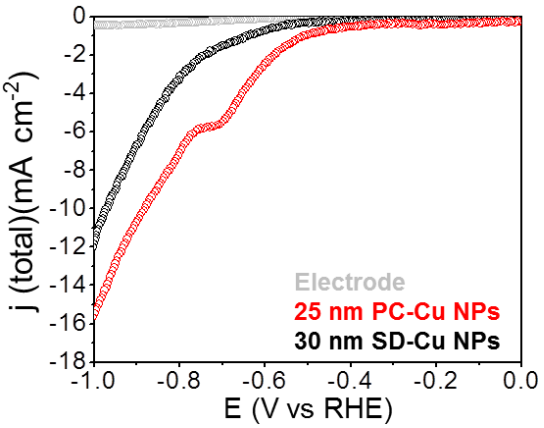

Figure S5. Geometric area normalized total current density.

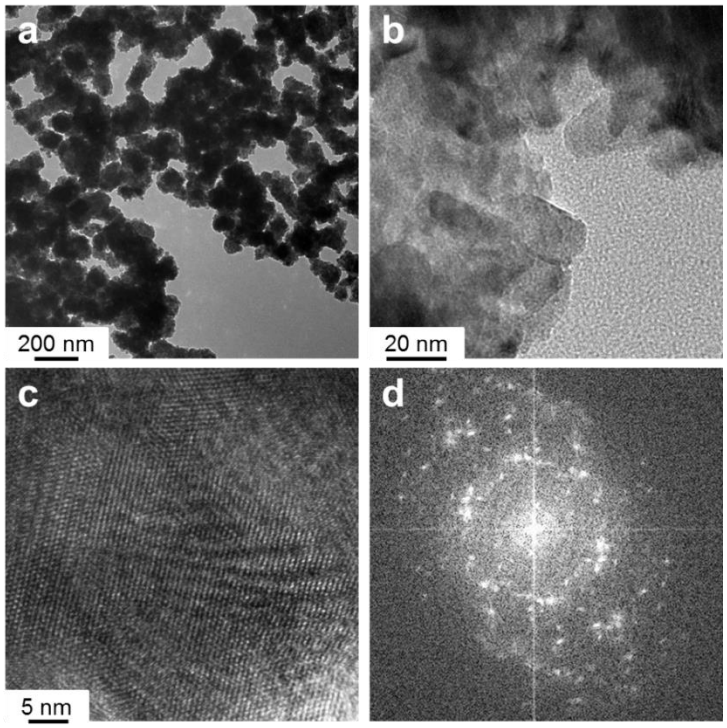

Figure S6. Polycrystalline structure of Cu NPs (PC-Cu NPs), (a), (b), (c) TEM images with increasing magnifications, (d) FFT image.

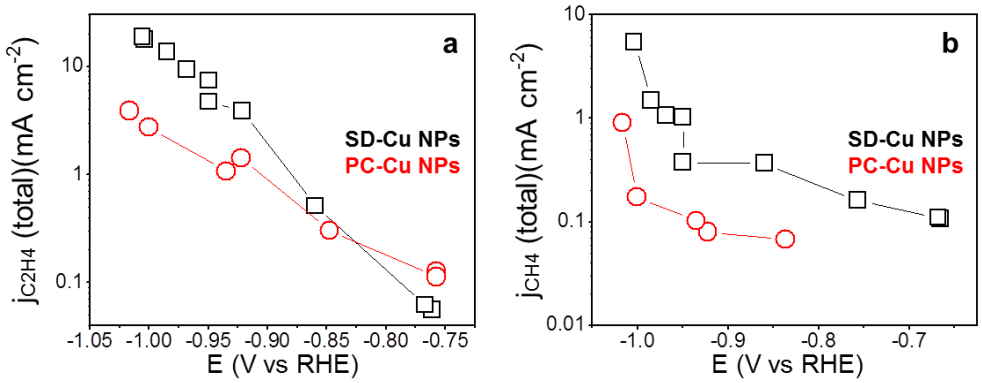

Figure S7. Partial current densities to CH_4 and C_2H_4, (a) C_2H_4 partial current densities, (b) CH_4 partial current densities.

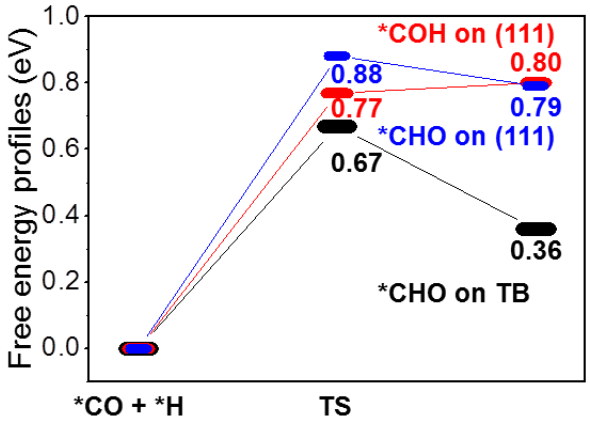

Figure S8. TS and formation energy of *COH on (111), *CHO on (111) and *CHO on TB. Data for *COH on (111), *CHO on (111) is literature data (ref 37).

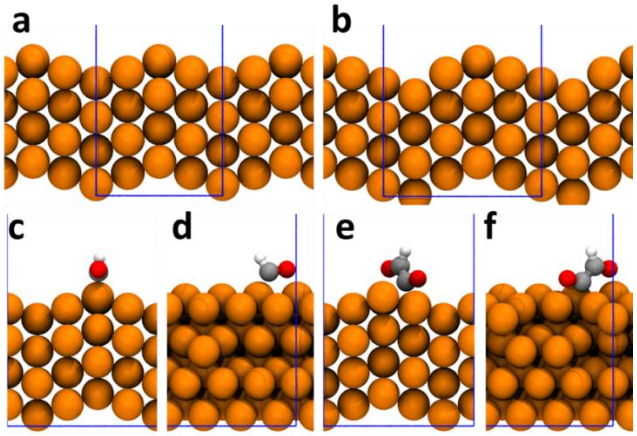

Figure S9. The atomic simulation model of (a) TB, (b) TB with stacking defect, (c) the optimized geometry of *CHO on TB from side view, (d) rotated by 90° along z-axis, (e) the optimized geometry of *OC-CHO on TB from side view, (f) rotated by 90° along z-axis.

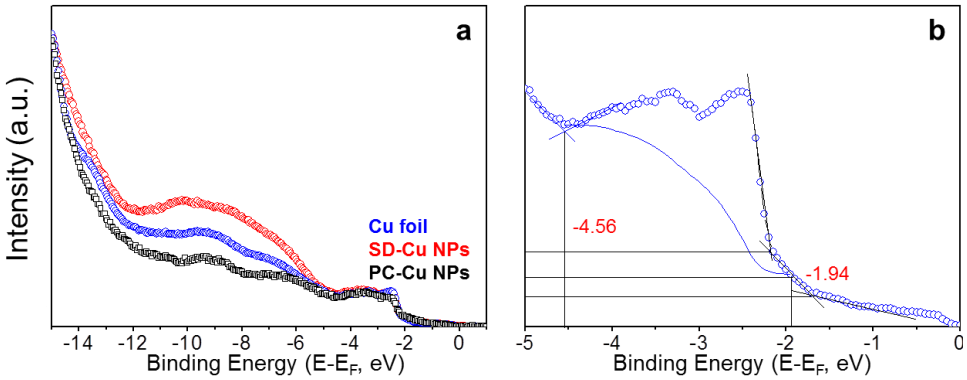

Figure S10. (a) entire UPS spectra measured for Cu(100) foil, SD-Cu NPs, and PC-Cu NPs, (b) d-band spectra of Cu(100) foil.

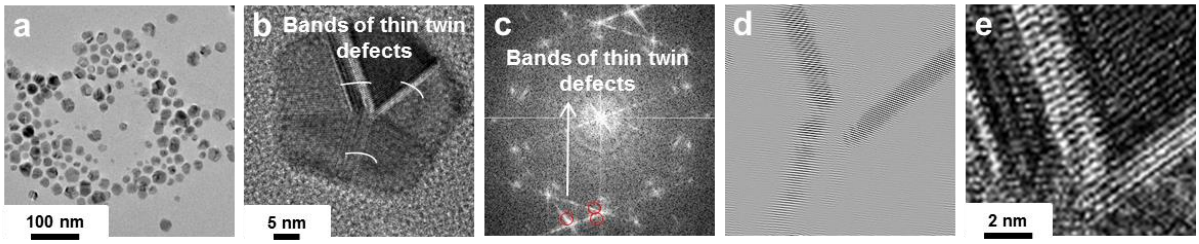

Figure S11. Analysis of SD-Cu NPs after electrochemical CO_2RR at -1 V for 1 hr, (a) low magnification TEM image of SD-Cu NPs after 1 hr, (b) HRTEM image of SD-Cu NPs after 1 hr, (c) FFT of SD-Cu NPs after 1 hr, (d) inverse FFT of SD-Cu NPs after 1 hr, (e) bands of twin defects after 1 hr.

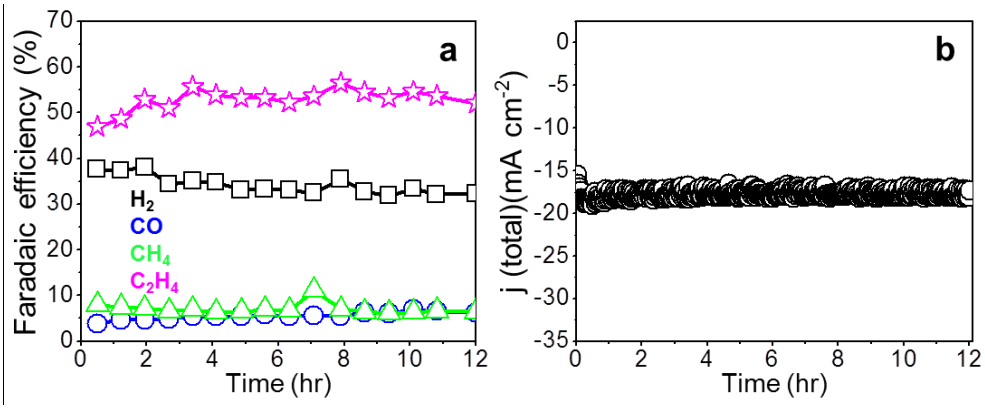

Figure S12. Stability test of SD-Cu NPs under -1 V (RHE) for 12 hr, (a) FE of SD-Cu NPs, (b) geometric area normalized current density of SD-Cu NPs.

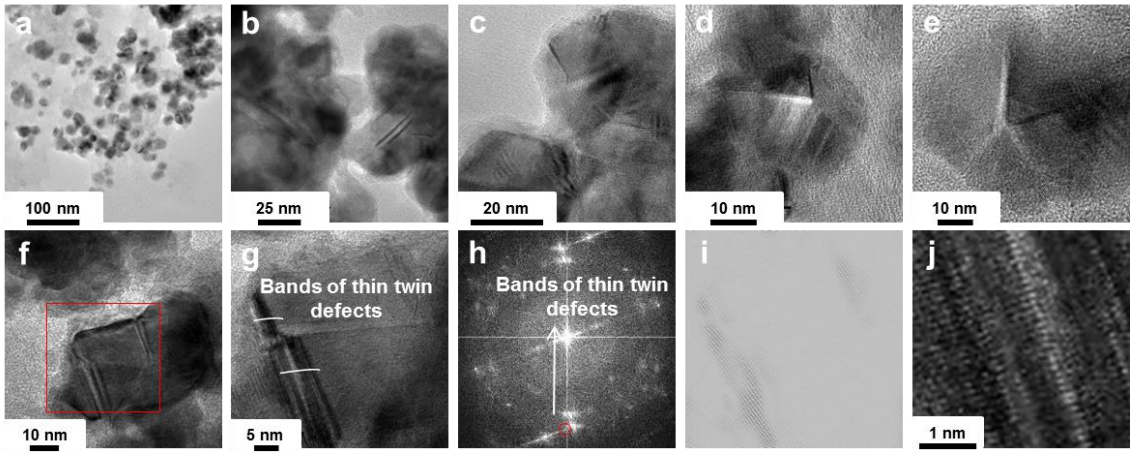

Figure S13. Analysis of SD-Cu NPs after electrochemical CO_2RR at -1 V for 12 hr, (a) low magnification TEM image of SD-Cu NPs after 12 hr, (b, c, d, e, f) HRTEM image of SD-Cu NPs after 12 hr, (g) HRTEM images of SD-Cu NPs after 12 hr (extending of a red box in Figure S13f), (h) FFT of SD-Cu NPs after 12 hr, (i) inverse FFT of SD-Cu NPs after 12hr, (j) bands of twin defects after 12 hr.

Table S1. FE for SD-Cu NPs

V [RHE]	H_2[%]	CO[%]	CH_4[%]	C_2H_4[%]	Ethanol[%]	Acetate[%]	Formate[%]	Total[%]
-0.664 ±0.00594	74.3±11.52	5.5±1.2	3.06±0.56	0	2.5	3.2	2.18	82.86±10.95
-0.759 ±0.00721	82.92±3.61	11.04±1.8	1.94±0.81	1.1±0.144	4.2	2.34	2.78	96.25±5.77
-0.85	58.38	17.03	4	5.56	0.04	0	0.02	84.97
-0.935 ±0.00167	59.93±11.12	16.50±3.51	2.76±1.56	28.42±5.82	0.03	0	0	107.61±6.87
-0.993 ±0.0129	33.47±4.76	6.79±3.03	6.58±1.99	52.43±2.72	0	0.5	0	97.63±5.86
-1.029 ±0.0178	29.62±8.8	4.96±2.03	7.81±4.314	51.98±3.72				91.78±10.41

Table S2. FE for PC-Cu NPs

V [RHE]	H_2[%]	CO[%]	CH_4[%]	C_2H_4[%]	Ethanol[%]	Acetate[%]	Formate[%]	Total[%]
-0.662 ±0.0136	80.74±11.78	9.75±1.29	0	0	0	0	8.14	98.63±12.75
-0.749 ±0.009	78.13±5.20	10.92±1.06	0	1.09±1.89	0.77	0.27	8.25	99.44±7.8
-0.83	80.17	11.93	0	5.91	0	0.46	13	111.47
-0.915 ±0.0128	56.46±3.90	13.60±4.76	0.761±0.88	14.21±9.88	2.3	1.44	6.3	95.09±11.6
-1.009 ±0.0113	39.08±10.05	8.21±4.83	6.99±5.15	37.08±6.87	2.14	6.54	1.5	101.54±9.8